



On the 3D printing of polypropylene and post-processing optimization of thermomechanical properties


Melanie Moczadlo, Department of Chemical and Biomolecular Engineering and Institute for Advanced Materials and Manufacturing, University of Tennessee, Knoxville, TN 37996, USA; Department of Materials Science and Engineering, University of Tennessee, Knoxville, TN 37996, USA

Qiyi Chen, Center for Nanophase Materials and Sciences, Oak Ridge National Laboratory, Oak Ridge, TN 37830, USA

Xiang Cheng, Department of Macromolecular Science and Engineering, Case Western Reserve University, Cleveland, OH 44106, USA

Zane J. Smith, Department of Chemical and Biomolecular Engineering and Institute for Advanced Materials and Manufacturing, University of Tennessee, Knoxville, TN 37996, USA; Department of Materials Science and Engineering, University of Tennessee, Knoxville, TN 37996, USA

Eugene B. Caldona, Department of Coatings and Polymeric Materials, North Dakota State University, Fargo, ND 58102, USA

Rigoberto C. Advincula , Department of Chemical and Biomolecular Engineering and Institute for Advanced Materials and Manufacturing, University of Tennessee, Knoxville, TN 37996, USA; Department of Materials Science and Engineering, University of Tennessee, Knoxville, TN 37996, USA; Center for Nanophase Materials and Sciences, Oak Ridge National Laboratory, Oak Ridge, TN 37830, USA; Department of Macromolecular Science and Engineering, Case Western Reserve University, Cleveland, OH 44106, USA

Address all correspondence to Rigoberto C. Advincula at radvincu@utk.edu

(Received 17 January 2022; accepted 19 January 2023; published online: 1 February 2023)

Abstract

Polypropylene (PP) is a highly desirable polyolefin in various plastic industries due to its outstanding thermomechanical properties and chemical resistance. Therefore, the 3D printing of PP is an interesting avenue to explore in digitized manufacturing, where more freedom in structural designs is available for new and extended applications, such as high-performance engineering parts. In this work, we 3D printed PP and studied the effect of printing parameters and post-processing conditions on the printed polymer's thermomechanical behavior. Results showed that nozzle and bed temperatures of 220 and 100°C produced a high printing quality. Infill percentages between 80 and 90%, coupled with a 4-h annealing at 110°C, also resulted in optimal printed properties. It is thought that PP can be potentially blended with polyethylene or other vinyl polymers for a more extended 3D printing utility and practical applications in rapid tooling and prototyping.

Introduction

Polyolefins are the most widely produced petroleum-based synthetic polymers. Besides their cost-effectiveness, they are desirable in many applications due to their durability, high flexibility, good chemical resistance, and thermal stability.^[1–3] Polypropylene (PP) and polyethylene (PE) are among the most commonly produced polyolefins, with more than 150 million metric tons of demand annually worldwide for various applications, including films, tubes, laminates, foams, packaging, and the like.^[4–6] PE has the simplest polyolefin structure, with ethylene as the monomer unit.^[7,8] Depending on the polymerization method, various grades of PE, such as low-density polyethylene (LDPE), high-density polyethylene (HDPE), and linear low-density polyethylene (LLDPE), to name a few, have several packaging and engineering applications.^[9] High-crystalline HDPE exhibits outstanding engineering properties and chemical resistance. At the same time, LDPE and LLDPE, due to

their soft polymer chains and branching, possess low hardness and strength but can also offer superb ductility, impact strength, and toughness that are good for packaging and plastic container fabrication. PP has a similar structure to PE, except for the presence of a pendant methyl group that determines the tacticity and crystallinity, which significantly affect the polymer's thermal properties.^[4,10] For instance, isotactic PP (iPP), with optimized structural symmetry, exhibits the highest crystallinity^[11] and melting point above 190°C, while a decrease in crystallinity to as low as 15% is expected for blended atactic PP (aPP).^[12,13] In general, compared to PE, PP displays better mechanical performance, thermal stability, and chemical resistance, heat deflection temperature (HDT) of 100°C at 0.46 MPa, tensile strength of 32 MPa, and flexural strength of 41 MPa.^[5] Although it has lower hardness and higher ductility and toughness than PE, PP is more useful in many engineering applications.

Additive manufacturing (AM) of PE and PP has been attracting significant attention owing to their utility in many practical applications and ready availability worldwide. AM (or 3D printing) has been important in manufacturing and prototyping for the past few years.^[14–20] 3D printing has the advantage of digitally creating more complex structures, which are not easily fabricated by traditional molding and tooling approaches. Among the various and most popular 3D printing techniques,

Melanie Moczadlo and Qiyi Chen have contributed equally to this work.

Rigoberto C. Advincula was an editor of this journal during the review and decision stage. For the MRS Communications policy on review and publication of manuscripts authored by editors, please refer to <http://www.mrs.org/editormanuscripts/>.

which include fused deposition modeling (FDM),^[21,22] stereolithography (SLA),^[23–25] direct ink writing (DIW),^[26–28] selective laser sintering (SLS),^[22,29,30] and inkjet printing,^[31] FDM is, by far, the most widely employed technique for printing thermoplastic polymers due to its cost-effectiveness, fast printing speed, and large-scale production capability.^[32,33]

FDM printing of PP and PE is highly desirable because of their many potential and promising industrial uses. However, PE is not easily 3D printed due to its high crystallinity and a high coefficient of thermal expansion (CTE), which often lead to a large volume shrinkage and warping during the printing process.^[34,35] These same properties make PE suitable for processing in injection, blow, compression molding, and other formative manufacturing methods but are considered weak in additive layering. On the other hand, pristine aPPs, aPP blends, and different tactic PPs have relatively low crystallinity, moderate CTE, and hardness and toughness adequate for material processing. Therefore, considering its inherent advantages and good 3D printability as a polyolefin material, exploring the utility of FDM and optimizing the printing parameters using PP as a feedstock material should be interesting.

We aim to demonstrate PP as a suitable substitute for PE in the 3D printing polyolefinic class of thermoplastics. We employed FDM to 3D print PP materials in this paper and optimized the corresponding printing conditions. We studied the influence of different printing parameters (e.g., infill volume, printing direction, and nozzle temperature) and post-processing procedures, such as annealing, on the printed polymer's thermomechanical performance. In addition, we characterized the composition of commercially available PP filaments.

Materials and methods

Materials

PP natural filaments, used for printing PP structures, were generously provided by Ultimaker and used as received. Magigoo adhesive was used to ensure sufficient adhesion of the printed parts on the build plate surface.

3D printing procedure

Ultimaker 2 + FDM printer was used in printing the PP filaments. The print speed was fixed at 25 mm s⁻¹ and layer height at 0.15 mm, while the nozzle and build plate temperatures were set at 220 and 100°C, respectively. Different infill densities of 20%, 50%, 70%, 80%, 90%, and 100% and printing angles of 0°, 30°, 45°, 60°, and 90° were used to study the resulting effect on the printed PP structures' mechanical properties. Magigoo was applied to the build plate before printing.

Annealing

Printed samples with 100% infill density were used for the annealing study to streamline the process. The printed samples

were annealed at 60, 80, 100, 110, 120, 130, 140, and 150°C for 4 h each. The annealing temperature providing the highest mechanical strength for the printed sample was selected for further additional annealing time frames of 1, 2, 8, and 12 h to study the correlation between the annealing time and mechanical properties.

Characterization

Thermogravimetric analysis (TGA) was performed on a Q50 thermogravimetric analyzer (TA Instruments), where 3D-printed samples were heated from 25 to 500°C under N₂ atmosphere at a heating rate of 10°C min⁻¹. Differential scanning calorimetry (DSC) was performed on a Q2000 differential scanning calorimeter (TA Instruments), where 6 mg of printed samples were heated from 25 to 200°C under N₂ atmosphere at a ramp rate of 10°C min⁻¹. Gas chromatography–mass spectrometry (GC–MS) pyrolysis was performed on an Agilent 5973 (Quantum Analytics) system with a Frontier Laboratories pyrolyzer. The multi-shot pyrolysis–gas chromatography/mass spectrometry (Py-GC/MS) was done by placing 0.2 mg of filament samples on a pyrolysis stainless-steel sample cup inserted into a micro-furnace. The characterization system consists of a micro-furnace multi-shot pyrolyzer EGA/Py-3030D (Frontier Lab, Japan) coupled with a gas chromatography–mass spectrometer (Agilent Technologies, 5973 inert mass selective detector, Quantum Analytics) through a longer metal column (Ultra ALLOY⁺-5, Frontier Laboratories). Pyrolysis was performed under a He flow of 1 mL min⁻¹, while the micro-furnace interface temperature was kept at 300°C. The GC oven temperature was initially set at 40°C and heated to 300 °C. All detected peaks were identified using the Frontier Laboratories and the National Institute of Standards and Technology (NIST) libraries.

An ASTM standard D638 tensile strength measurement was done on a Liyi Tech LY-1065A universal testing machine (UTM) at a pull rate of 10 mm min⁻¹. Type V tensile bars were used with dimensions according to ASTM D638 standards.

Results and discussion

The PP filament was first characterized to study its properties and confirm the presence of any additives or blend compositions. The DSC curve of the as-received PP filament is shown in Fig. 1(a), where a single melting peak can be observed at 136 °C. The melting started at 97.3 °C and ended at 144.8 °C. By integrating the melting peak in this temperature range and using the theoretical value of 100% isotactic PP's heat of fusion value of 178 J g⁻¹,^[36] the percent crystallinity was determined as 21.9%. On the other hand, Fig. 1(b) displays the TGA curve of the as-received PP filament, showing an onset degradation at 334 °C and 2.45% char yield at 500 °C, both of which are in good agreement with the thermal properties of PP reported in the literature.^[37] The char yield may be due to inorganic fillers or other additives, which serve as processing aids and stabilizers during filament fabrication from PP pellets.

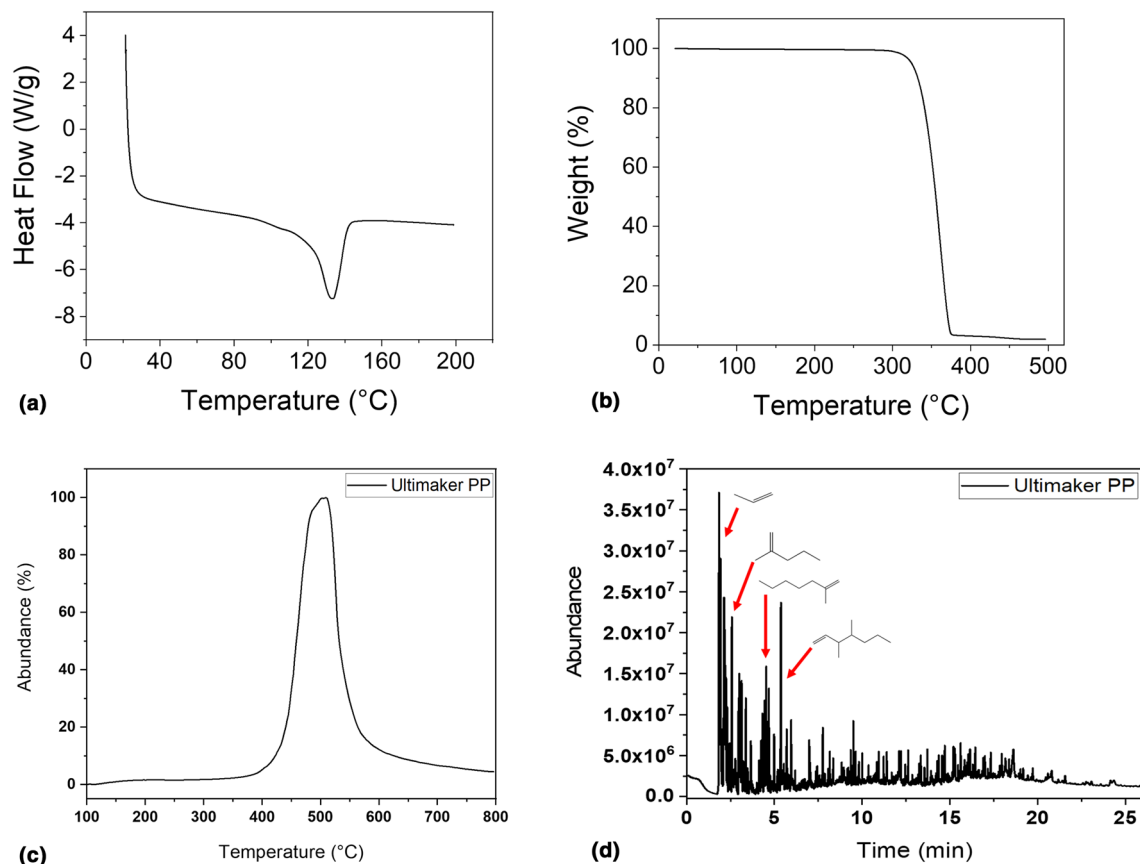


Figure 1. (a) DSC curve, (b) TGA curve, (c) evolved gas analysis (EGA)-MS, and (d) multi-shot Py-GC/MS of PP filament.

Py-GC/MS was performed to confirm the structural identity and composition of the PP filament. The thermogram of the PP filament [Figure 1(c)] showed an onset degradation near 400°C, indicating its relatively higher thermal stability, but also comparable to the TGA result. A small peak, centered at around 325 m/z, is due to the epoxy resin diglycidyl ether of bisphenol A (DGEBA). This additive may have been used in PP filament fabrication. Further details on the thermogram of PP and its additives are shown in Figures S1 and S2. The pyrolyzed filament material at 700 °C was delivered through the GC/MS system, and the resulting stable chemical fragments were assigned according to the major peaks of the pyrogram as shown in Figure 1(d). These peaks indicate the identity of the PP filament, and the thermal decomposition was mainly due to the scission of the backbone C–C bonding. Note that no attempt was made to completely reverse engineer this commercial PP material, and the characterization was performed to confirm the structure and composition of the commercial PP filament.

We also explored the different 3D printing conditions for processing the PP natural filament using the Ultimaker 2+ printer. The print speed was fixed at 25 mm s⁻¹ and layer height at 0.15 mm. Wall thickness corresponded closer to the original nozzle diameter of 2.8 mm. We printed other PP structures employing nozzle temperatures between 150 and

230°C and bed (build plate) temperatures from 60 to 110°C and found that a successful print with high resolution can be achieved using nozzle and bed temperatures above 220 and 100°C, respectively. To reduce the materials consumption and streamline the overall process, neat PP tensile bars in X orientation were printed in cubic and grid infill patterns at different infill densities (percentages) and their measured mechanical strength was used to determine the optimal nozzle temperature. These results show that at the specified peak temperatures, the printed layers have reached their maximum bonding strength. Hence, to streamline our discussion, we considered 220°C as the optimum nozzle temperature and used it, not only to print Y and Z orientations but also to advance with detailed investigation throughout this study. Considering the relatively low melting point of PP (i.e., 144.8°C), the high printing temperature of PP ensures complete melting, smooth filament extrusion, and adequate adhesion strength between the printed layers, thereby overcoming the processability challenge caused by the polymer's high crystallinity and high viscosity. To further demonstrate the printability of PP, we printed a blind valence clip [Fig. 2(a)] with a broader overlayer on a build plate. This was actually redrawn from an original failed part which was made of polystyrene (PS). This printing procedure minimizes the possibility of print delamination during fabrication. The

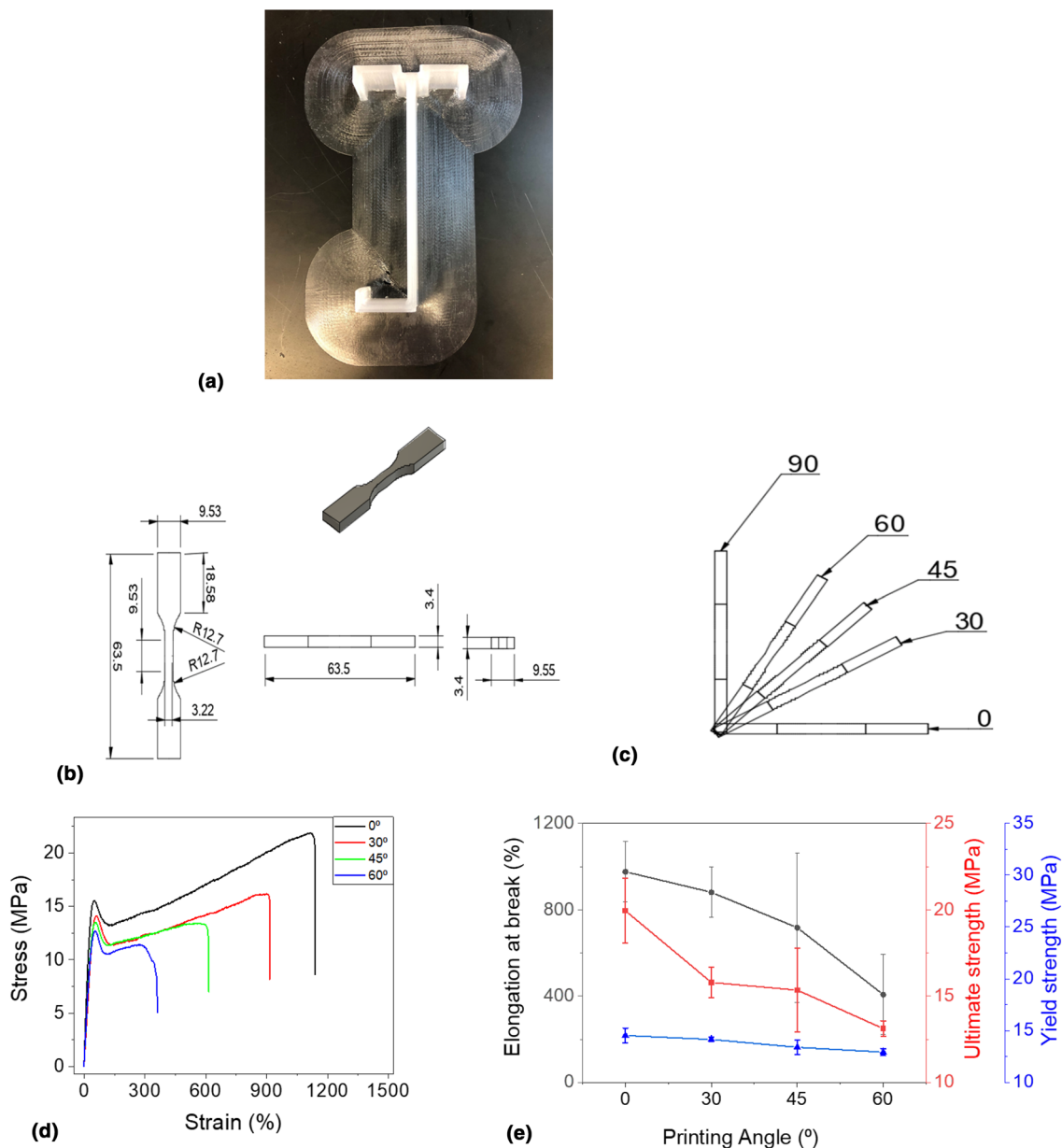


Figure 2. Effect of printing orientation on mechanical properties. (a) 3D-printed blind clip using optimized printing conditions. (b) Tensile bar dimensions in mm. (c) 0° to 90° printing angles. (d) Stress–strain curves and (e) elongation at break and ultimate yield strength of tensile bar specimens printed using different printing angles.

corresponding cross-section SEM image of 3D-printed PP is shown in Figure S3. It can be seen that using the optimized printing conditions, the gaps and voids between the printed layers are minimal. This result is consistent with what has been observed for the role of temperature in melt flow viscosity from both the nozzle and build plate layering.^[38] To increase adhesion at the interface between the prints and the bed, several adhesives were used. Magigoo displayed the best result, while the other adhesives provided poor adhesion, leading to early delamination of the prints from the bed during printing. The use of adhesive is important as print delamination is a common

source of print failures and screws up the programmed x–y–z scale correlation from computer-aided design (CAD) to slicing, the result of which is shown in the failed prints in Figure S4.

To study the effect of different processing conditions on the mechanical performance of PP, we printed ASTM standard tensile specimens for tensile testing. The dimensions of the printed specimens are shown in Fig. 2(b). First, we studied the effect of different printing angles (i.e., 0°, 30°, 45°, 60°, and 90°), as illustrated in Fig. 2(c), on the mechanical properties of the printed specimens. We observed that the 90° printing orientation resulted in many loose filaments at the top end of the

printed specimens (Fig. S4). This result may have been caused by frequent sample shaking, while the topmost layer is printed, leading to disordered layer formation. Therefore, the 90°-oriented printed samples were not characterized herein. The tensile test results for samples printed in 0°, 30°, 45°, and 60° orientations are plotted in Fig. 2(d) and (e), where a decrease in mechanical performance with increasing printing angles can be observed: elongation at break from 976 to 407%, ultimate strength from 20 to 13.1 MPa, and yield strength from 14.5 to 12.9 MPa. Since the perpendicularity of the printed layers to the specimen's longitudinal axis increases with the printing angles, the printed layers experience increased separation force from each other, resulting in decreased interlayer adhesion and overall mechanical integrity.

The effect of different infill densities (i.e., 20%, 50%, 70%, 80%, 90%, and 100%) on the mechanical performance of the printed PP samples was also studied. For each infill density, 10-PP specimens were printed and tested. To streamline the process, all specimens were printed at 0°-printing orientation. The resulting stress–strain curves at different infill densities are shown in Fig. 3(a), while the ultimate strength, yield strength, and elongation at break are plotted in Fig. 3(b). When infill density increases from 20 to 70%, increasing mechanical performance can be observed. Higher infill densities result in more compact materials capable of withstanding greater external loads.

Interestingly, the mechanical performance remained nearly constant from 70 to 90% infill density while decreasing considerably at 100% infill density, where the elongation at break decreased from roughly 1400% to less than 1000%. This can imply that thermal expansion (and shrinkage) effect based on the coefficient of thermal expansion is still a strong consideration. (PP is between 6.0 and 17.0 ($10^{-5}/^{\circ}\text{C}$)). Ideally, printed materials' infill density should conform with those set in the software and printing program. However, it has been observed that the actual infill density in the printed sample increases rapidly with increasing input infill density (i.e., from 20 to 70%) in the software while increasing moderately for input infill density of 70% to 100%. Meanwhile, during the filament extrusion

from the nozzle, the die swell effect causes the extruded filament to be wider and thicker than the gap generated by the slicing software. Thus, the extra extruded material adds to the programmed gap between the filaments (i.e., at the infill density from 70 to 90%). When the infill density reaches 100%, the software generates no gap between the printed filaments. Therefore, the die swell effect leads to an overflow, compromising the infill packing order and lowering the mechanical integrity. This phenomenon also widens the fidelity of the actual printed dimensions versus the original CAD dimensions. This implies that for PP, it is possible to achieve the desired properties and function of the printed part beginning at 70% infill density. The final material properties should then take into account: (1) the melt extrusion behavior, (2) the quenching mechanism to solid state, (3) the equilibrium properties (addressed by annealing), and (4) the geometry and volume of the printing. This, however, does not necessarily apply to other polymers, including popular FDM thermoplastic filaments such as poly(acrylonitrile butadiene styrene) (ABS) and polylactic acid (PLA) and can largely be a function of their semi-crystallinity and other thermal or enthalpic properties. In principle, paying close attention to these factors could result in material costs and printing time savings. Again, as a class of polyolefins, PP is more practical than other polymers like PE since the former's CTE results in less warping and delamination and prevents early printing failure. In general, PP/PE blends or copolymers and using PP with different tacticity may help broaden the properties and processing windows for polyolefins.

The post-processing procedure plays a vital role in further enhancing the mechanical properties of thermoplastic polymers, especially for those with crystalline structures. We annealed our 3D-printed PP samples at varying times and using different temperatures to strengthen their equilibrium properties further. First, stress–strain curves at different annealing times at 100°C were measured. The elongation at break and ultimate and yield strength of PP samples annealed at different times at 60 °C. The changes were not noticeable over the sampling of the thermomechanical properties even up to 12 h at this temperature. However, the changes are more noticeable with increasing

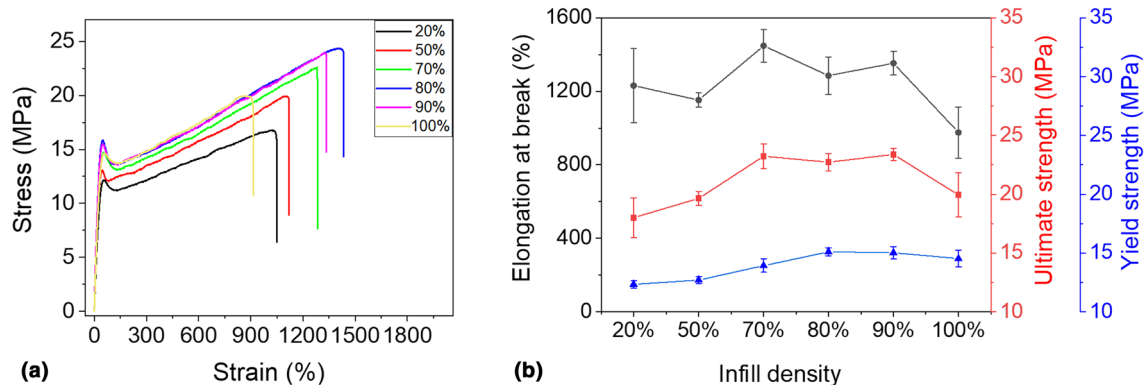


Figure 3. (a) Stress–strain curves and (b) elongation at break and ultimate yield strength of printed PP specimens at different infill densities.

temperatures especially beyond 80 °C. We first set the annealing time to 4 h and tested 7 annealing temperatures below the melting point but above the glass transition temperature (T_g): 60, 80, 100, 110, 120, 130, and 140°C. The tensile test results at different annealing temperatures are shown in Figs. 4(a), S5; after annealing at 60°C, the elongation at break and ultimate strength increased from 976 to 1236% and 19.9 to 23.3 MPa,

respectively. This result indicates a possible rearrangement of PP segments into a more crystalline structure, which improves the mechanical strength, even at a low annealing temperature of 60 °C. Between annealing temperatures of 60 to 100°C, no significant mechanical property change is observed, indicating the stability of chain arrangement at this temperature range. When the annealing temperature was increased from 100 to 130°C,

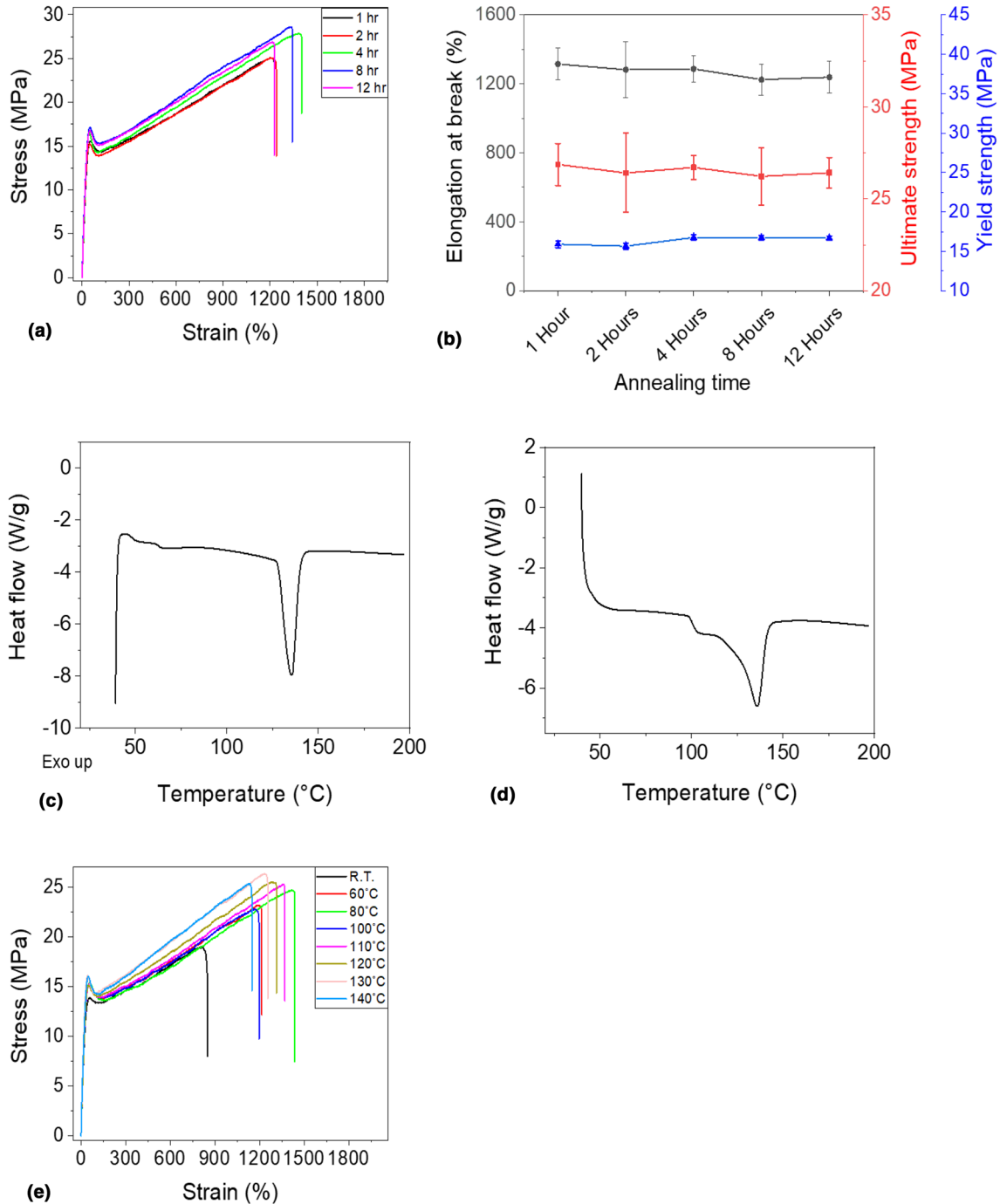


Figure 4. Tensile test data of PP specimens with different annealing conditions. (a) Stress–strain curves at different annealing times at 100°C. (b) Elongation at break and ultimate and yield strength of PP samples annealed at different times at 60 °C. The DSC curves of 3D-printed PP annealed are shown at (c) 100°C and (d) 130 °C. (e) Stress–strain curves at different annealing temperatures at 4 h each.

an increase in elongation at break from 1191 to 1346%, and ultimate strength from 13.26 to 26.7 MPa was observed, this improvement may be caused by further rearrangement of the PP chains at temperatures above 100°C, forming higher crystalline structures and closer to equilibrium. The observation is important as it points to a multiple of factors that can be affected by the quenching behavior of the melt and the packing of the extruded lines during printing. This range of favorable annealing temperatures establishes conditions closer to equilibrium as autohesion (movement of the chains toward equilibrium) (Figure S6) or removal of the residual stress added during printing occurs. To corroborate this hypothesis, we performed DSC on the samples annealed at 100 and 130°C, as shown in Fig. 4(c), (d). The percentage crystallinity values calculated from the DSC curves are 21.9%, 23.6%, and 25.7% for unannealed and annealed samples at 100 and 130°C for 4 h, respectively. The increase in crystallinity for annealed samples confirms chain rearrangement into a more crystalline PP structure or, perhaps, another phase (e.g., polymorph), resulting in improved mechanical strength. However, when the annealing temperature was increased further to 140 °C, the ultimate and yield strength and the elongation at break slightly decreased (Figure S5). We attribute this mechanical property loss to possible slight degradation of the polymer at 140 °C. Therefore, 110 °C was chosen as the annealing temperature for varying annealing times of 1, 4, 8, and 12 h, and the tensile test results shown in Figures 4(b) and S5 (elongation at break and ultimate and yield strength of PP samples annealed at different temperatures). The ultimate and yield strength and elongation at break remained nearly constant, except for some small changes, indicating that the rearrangement of the segmental chain may likely have been completed within 1 h, thus increasing the annealing time does not lead to further structural change or property improvement. Overall, these post-processing condition optimization studies can help minimize the project duration and the cost of manufacturing mechanically improved PP-based materials in future.

Conclusion

We have successfully printed commercially available PP filaments with optimized printing conditions, nozzle temperature of 220 °C, and bed temperature of 100°C, with improved bed adhesion, resulting in high printing quality and thermomechanical performance. We studied the effect of different processing conditions on mechanical properties, including printing angles, infill density, annealing temperatures, and annealing time. Results showed that a mechanically improved printed PP structure requires infill densities ranging from 80 to 90% and an ideal annealing temperature of 110°C for 4 h. Polyolefins, such as PP, are an essential class of widely available thermoplastic polymers and promising for applications in the AM field. For any AM study on polymer filaments, it is necessary to conduct printing optimization experiments to develop printed polymer structures with robust thermo-physical properties. Overall, our research can set a modus operandi for setting standardized and

optimized printing and processing for polyolefinic and other thermoplastic materials and realize their utility in producing mechanically stable AM parts rather than parts fabricated via traditional formative manufacturing methods.

Acknowledgments

The authors gratefully acknowledge funding from the Governor's Chair Funds, the University of Tennessee System, and the Center for Materials Processing (CMP)-TCE. Technical support from Malvern Panalytical, Frontier Laboratories and Quantum Analytics are also acknowledged. Work (or part of this work) was conducted by ORNL's Center for Nanophase Materials and Sciences by RCA, a US Department of Energy Office of Science User Facility.

Data availability

Additional data are available with the supplementary information file that will be made accessible with publication. In addition, more data and inquiry are possible through communication with the authors.

Declarations

Conflict of interest

On behalf of all authors, the corresponding author states that there is no conflict of interest.

Supplementary Information

The online version contains supplementary material available at <https://doi.org/10.1557/s43579-023-00329-2>.

References

1. M. Tolinski, *Additives for Polyolefins: Getting the Most Out of Polypropylene, Polyethylene and TPO* (William Andrew, Oxford, 2015)
2. N.K. Boalen, M.A. Hillmyer, Post-polymerization functionalization of polyolefins. *Chem. Soc. Rev.* **34**(3), 267 (2005)
3. A. Ammala, S. Bateman, K. Dean, E. Petinakis, P. Sangwan, S. Wong, Q. Yuan, L. Yu, C. Patrick, K. Leong, An overview of degradable and biodegradable polyolefins. *Prog. Polym. Sci.* **36**(8), 1015 (2011)
4. J. Gulmine, P. Janissek, H. Heise, L. Akcelrud, Polyethylene characterization by FTIR. *Polym. Test.* **21**(5), 557 (2002)
5. F. Padden Jr., H. Keith, Spherulitic crystallization in polypropylene. *J. Appl. Phys.* **30**(10), 1479 (1959)
6. E.B. Caldona, J.M.C. Albayalde, A.M.P. Aglosolos, K.S. Bautista, M.D. Tavora, S.A.P. Cabalza, J.R.O. Diaz, M.D. Mulato, Titania-containing recycled polypropylene surfaces with photo-induced reversible switching wettability. *J. Polym. Environ.* **27**(7), 1564 (2019)
7. A. Peacock, *Handbook of Polyethylene: Structures: Properties, and Applications* (CRC Press, Boca Raton, 2000)
8. A.-C. Albertsson, S.O. Andersson, S. Karlsson, The mechanism of biodegradation of polyethylene. *Polym. Degrad. Stab.* **18**(1), 73 (1987)
9. J.D. Burguillos, E.B. Caldona, Design and development of a novel waste container from HDPE-layered bins. *J. King Saud Univ. Eng. Sci.* **32**(1), 85 (2020)

10. N. Pasquini, A. Addeo, *Polypropylene Handbook* (Hanser Publishers, Munich, 2005)
11. G. Natta, P. Corradini, *Stereospecific Polymers* (Elsevier, Amsterdam, 1967), pp.743–746
12. P. Choi, W. Mattice, Molecular origin of demixing, prior to crystallization, of atactic polypropylene/isotactic polypropylene blends upon cooling from the melt. *J. Chem. Phys.* **121**, 8647 (2004)
13. J. Chen, F. Tsai, Y. Nien, P. Yeh, Isothermal crystallization of isotactic polypropylene blended with low molecular weight atactic polypropylene Part I. Thermal properties and morphology development. *Polymer* **46**(15), 5680 (2005)
14. A. Dawood, B.M. Marti, V. Sauret-Jackson, A. Darwood, 3D printing in dentistry. *Br. Dent. J.* **219**(11), 521 (2015)
15. Z. Chen, Z. Li, J. Li, C. Liu, C. Lao, Y. Fu, C. Liu, Y. Li, P. Wang, Y. He, 3D printing of ceramics: a review. *J. Eur. Ceram. Soc.* **39**(4), 661 (2019)
16. N. Shahrudin, T.C. Lee, R. Ramlan, An overview on 3D printing technology: technological, materials, and applications. *Procedia Manuf.* **35**, 1286 (2019)
17. R.C. Advincula, J.R.C. Dizon, E.B. Caldon, R.A. Viers, F.D.C. Siacor, R.D. Maalihan, A.H. Espera, On the progress of 3D-printed hydrogels for tissue engineering. *MRS Commun.* **11**(5), 539 (2021)
18. J.R.H.S. Agueda, Q. Chen, R.D. Maalihan, J. Ren, Í.G. da Silva, N.P. Dugos, E.B. Caldon, R.C. Advincula, 3D printing of biomedically relevant polymer materials and biocompatibility. *MRS Commun.* **11**, 197 (2021)
19. A.C.C. de Leon, Í.G. da Silva, K.D. Pangiliinan, Q. Chen, E.B. Caldon, R.C. Advincula, High performance polymers for oil and gas applications. *React. Funct. Polym.* **162**, 104878 (2021)
20. D.B. Gutierrez, E.B. Caldon, R.D. Espiritu, R.C. Advincula, The potential of additively manufactured membranes for selective separation and capture of CO₂. *MRS Commun.* **11**(4), 391 (2021)
21. Q. Chen, J.D. Mangadiao, J. Wallat, A. De Leon, J.K. Pokorski, R.C. Advincula, 3D printing biocompatible polyurethane/poly (lactic acid)/graphene oxide nanocomposites: anisotropic properties. *ACS Appl. Mater. Interfaces* **9**(4), 4015 (2017)
22. A.C. de Leon, Q. Chen, N.B. Palaganas, J.O. Palaganas, J. Manapat, R.C. Advincula, High performance polymer nanocomposites for additive manufacturing applications. *React. Funct. Polym.* **103**, 141 (2016)
23. V.S. Voet, T. Strating, G.H. Schmelting, P. Dijkstra, M. Tietema, J. Xu, A.J. Woortman, K. Loos, J. Jager, R. Folkersma, Biobased acrylate photocurable resin formulation for stereolithography 3D printing. *ACS Omega* **3**(2), 1403 (2018)
24. J.Z. Manapat, Q. Chen, P. Ye, R.C. Advincula, 3D printing of polymer nanocomposites via stereolithography. *Macromol. Mater. Eng.* **302**(9), 1600553 (2017)
25. R.D. Maalihan, Q. Chen, J.R.H.S. Agueda, B.B. Pajarito, H. Tamura, R.C. Advincula, On the use of surfactant-complexed chitosan for toughening 3D printed polymethacrylate composites. *Macromol. Mater. Eng.* **306**(1), 2000448 (2021)
26. X. Wan, L. Luo, Y. Liu, J. Leng, Direct ink writing based 4D printing of materials and their applications. *Adv. Sci.* **7**(16), 2001000 (2020)
27. Q. Chen, P. Cao, R.C. Advincula, Mechanically robust, ultraelastic hierarchical foam with tunable properties via 3D printing. *Adv. Funct. Mater.* **28**(21), 1800631 (2018)
28. Q. Chen, J. Zhao, J. Ren, L. Rong, P. Cao, R.C. Advincula, 3D printed multifunctional, hyperelastic silicone rubber foam. *Adv. Funct. Mater.* **29**(23), 1900469 (2019)
29. A. Awad, F. Fina, A. Goyanes, S. Gaisford, A.W. Basit, 3D printing: Principles and pharmaceutical applications of selective laser sintering. *Int. J. Pharm.* **586**, 119594 (2020)
30. A.H. Espera Jr., A.D. Valino, J.O. Palaganas, L. Souza, Q. Chen, R.C. Advincula, 3D Printing of a robust polyamide-12-carbon black composite via selective laser sintering: thermal and electrical conductivity. *Macromol. Mater. Eng.* **304**(4), 1800718 (2019)
31. L. Wu, Z. Dong, F. Li, H. Zhou, Y. Song, Emerging progress of inkjet technology in printing optical materials. *Adv. Opt. Mater.* **4**(12), 1915 (2016)
32. A.D. Valino, J.R.C. Dizon, A.H. Espera Jr., Q. Chen, J. Messman, R.C. Advincula, Advances in 3D printing of thermoplastic polymer composites and nanocomposites. *Prog. Polym. Sci.* **98**, 101162 (2019)
33. J.R.C. Dizon, A.H. Espera Jr., Q. Chen, R.C. Advincula, Mechanical characterization of 3D-printed polymers. *Addit. Manuf.* **20**, 44 (2018)
34. A. Gudadhe, N. Bachhar, A. Kumar, P. Andrade, G. Kumaraswamy, Three-dimensional printing with waste high-density polyethylene. *ACS Appl. Polym. Mater.* **1**(11), 3157 (2019)
35. D. Filgueira, S. Holmen, J.K. Melbø, D. Moldes, A.T. Echtermeyer, G. Chinga-Carrasco, 3D printable filaments made of biobased polyethylene biocomposites. *Polymers* **10**(3), 314 (2018)
36. C. Minogianni, K.G. Gatos, C. Galiotis, Estimation of crystallinity in isotropic isotactic polypropylene with Raman spectroscopy. *Appl. Spectrosc.* **59**(9), 1141 (2005)
37. K. Lau, P. Hung, M.-H. Zhu, D. Hui, Properties of natural fibre composites for structural engineering applications. *Composite B* **136**, 222 (2018)
38. F.D.C. Siacor, Q. Chen, J.Y. Zhao, L. Han, A.D. Valino, E.B. Taboada, E.B. Caldon, R.C. Advincula, On the additive manufacturing (3D printing) of viscoelastic materials and flow behavior: from composites to food manufacturing. *Addit. Manuf.* **45**, 102043 (2021)

Publisher's Note Springer Nature remains neutral with regard to jurisdictional claims in published maps and institutional affiliations.

Springer Nature or its licensor (e.g. a society or other partner) holds exclusive rights to this article under a publishing agreement with the author(s) or other rightsholder(s); author self-archiving of the accepted manuscript version of this article is solely governed by the terms of such publishing agreement and applicable law.